Journal of Engineering Science *Vol. XXXIII, no. 1 (2026), pp. 8 - 20*
Fascicle *Industrial Engineering* *ISSN 2587-3474*
Topic *Mechanical Engineering and Technologies* *eISSN 2587-3482*

https://doi.org/10.52326/jes.utm.2026.33(1).01
UDC 621.67:532.5:004.94

APPLICATION OF FLUID-STRUCTURE INTERACTION SIMULATIONS IN THE OPTIMISATION CYCLE OF CENTRIFUGAL PUMP IMPELLERS

Viorel Bostan[1], ORCID: 0000-0002-2422-3538,
Andrei Petco[1,2*], ORCID: 0009-0004-0577-3296,
Dumitru Odainîi[1], ORCID: 0000-0001-6587-6247,
Dmitrii Croitor[1], ORCID: 0009-0005-9033-8543,
Vadim Zubac[1], ORCID: 0009-0002-5003-0729,
Nadejda Proca[1,2], ORCID: 0009-0004-7854-7599

[1]Technical University of Moldova, 168 Stefan cel Mare Blvd., Chisinau, MD-2004, Republic of Moldova
[2]S.R.L. "CRIS" 68/2-69 Albisoara str., Chisinau, MD-2005, Republic of Moldova,
* Corresponding author: Andrei Petco, *andrei.petco@if.utm.md*

Received: 12. 18. 2025
Accepted: 22. 01. 2026

Abstract. The integration of fluid-structure interaction (FSI) simulations into the design cycle of centrifugal pump impellers is an important part of this methodology, ensuring the safe conduct of bench tests. This study evaluates the behaviour of the CH 100/32-11-1 pump impeller using a combined numerical workflow involving ANSYS CFX and Mechanical. After a thorough analysis of mesh convergence, the hydraulic loads obtained from Computational Fluid Dynamics (CFD) data were transferred to the structural domain for quantitative assessment of equivalent stresses and strains. The analysis shows that the maximum equivalent stress for the optimised geometry is 24.45 MPa, which is within the tensile strength limit of PA12, confirming the feasibility of manufacturing a functional prototype using a Selective Laser Sintering (SLS). A comparative assessment with respect to the CH 6.3/20-1.1-2 and CH 100/125-75-5 models shows a non-linear scaling of structural loads, with the latter demonstrating critical failure stresses (51.7 MPa) exceeding the material's strength limits. The results confirm that the Fluid-Structure Interaction (FSI) numerical model is an important filter in the preparation stage for prototyping turbomachinery components using additive technologies.

Keywords: *Additive Manufacturing, Centrifugal pump, impeller, Computational Fluid Dynamics, Fluid-Structure Interaction.*

Rezumat. Integrarea simulărilor de interacțiune fluid-structură (FSI) în ciclul de proiectare al rotoarelor pompelor centrifuge este o parte importantă a acestei metodologii, asigurând efectuarea în siguranță a testelor pe banc de încercare. Acest studiu evaluează comportamentul rotorului pompei CH 100/32-11-1 utilizând un flux de lucru numeric combinat care implică ANSYS CFX și Mechanical. După o analiză amănunțită a convergenței plasei, încărcările hidraulice obținute din datele de Dinamică Computațională a Fluidelor (CFD) au fost transferate în domeniul structural pentru evaluarea cantitativă a tensiunilor și deformărilor echivalente. Analiza arată că tensiunea echivalentă maximă pentru geometria

optimizată este de 24,45 MPa, ceea ce se încadrează în limita de rezistență la tracțiune a PA12, confirmând fezabilitatea fabricării unui prototip funcțional utilizând sinterizarea selectivă cu laser (SLS). O evaluare comparativă în raport cu modelele CH 6.3/20-1.1-2 și CH 100/125-75-5 arată o scalare neliniară a încărcărilor structurale, acesta din urmă demonstrând tensiuni critice de rupere (51,7 MPa) care depășesc limitele de rezistență ale materialului. Rezultatele confirmă faptul că modelul numeric de interacțiune fluid-structură (FSI) este un filtru important în etapa de pregătire pentru prototiparea componentelor turbomașinilor folosind tehnologii aditive.

Cuvinte cheie: *fabricație aditivă, pompă centrifugă, rotor, dinamică computațională a fluidelor, interacțiune fluid-structură.*

1. Introduction

Centrifugal pumps are one of the most widely used types of pumps, serving as the primary means of transporting a wide range of liquids in various operating and outdoor conditions in industries such as chemical and petrochemical, food, pharmaceutical industry, food industry, mining [1] , energy sector [2,3] , as well as in areas such as water supply [4,5], wastewater treatment and agricultural irrigation. This type of pump is also quite common in the transport sector, from automotive and rail transport [6] to the aerospace industry [7].

It should also be noted that, in the context of the global drive for energy efficiency and carbon footprint reduction, many countries are setting targets for improving energy efficiency. The current global drive for economic efficiency and environmental sustainability is clearly reflected in the 2015 Paris Agreement on climate change. In order to fulfil the commitments made by the EU under this agreement, a number of measures have been taken, including a commitment by EU governments to pay particular attention to energy efficiency and to set a target of increasing energy efficiency by at least 32.5% by 2030 (compared to 2020) [8,9].

These commitments are forcing manufacturers [10,11], including centrifugal pump manufacturers, to optimise the design of their equipment [12,13]. Thus, the optimisation of centrifugal pump flow parts has evolved from a purely engineering task into an economic and environmental requirement. According to the American Hydraulic Institute, pumps account for up to 20% of energy consumption in developed countries [14,15] . At the same time, a life cycle cost (LCC) analysis of pump units shows that the initial capital costs of purchasing equipment account for only about 10-15% of total costs, with the rest being energy and maintenance costs [15]. The problem of optimising the flow parts of pumps, primarily the impellers, is a pressing one, and even a slight increase in hydraulic efficiency at the design and optimisation stage of the impeller design can lead to significant long-term resource savings, offsetting the operating costs associated with energy consumption.

However, the problem of optimisation is not limited to energy performance. Modern operating conditions often force pump units to operate in modes that are far from the Best Efficiency Point (BEP), which leads to the occurrence of unsteady hydraulic phenomena such as reverse currents, vortex formation in inter-blade channels and cavitation [16–18]. These processes not only reduce the energy efficiency, but also generate intense pressure pulsations, causing increased vibration and fatigue wear of structures.

Traditional design methodologies based on empirical data [19,20], combined with iterative testing of physical prototypes, are inefficient due to their labour intensity and long development times. The geometry of the impeller is characterised by a number of interrelated

variables, including blade angles β, meridional section shape, etc., which in turn means that changing any of these factors leads to a non-linear response of the system, making impeller modelling in modern conditions extremely difficult without the use of CFD simulations.

Since the application of direct optimisation methods in conjunction with CFD calculations requires significant computing power and cannot be performed with a large number of geometric parameters, surrogate modelling methods such as the Kriging method [21], artificial neural networks (ANN) [22] and methods based on the Response Surface Methodology (RSM) [23–25] have become widely used. The construction of a response surface allows the dependence of target functions on geometric parameters to be approximated, after which a global search for the optimum is carried out using stochastic optimisation algorithms, such as genetic (evolutionary) algorithms, for example NSGA-II [5,26,27].

Despite the widespread use of this class of pumps [19], conditions at customer facilities and in the systems that serve them dictate operating requirements that often cannot be predicted by classical models [19,28] of materials science and hydrodynamics, which often leads to significant deviations from the parameters in BEP. Under extreme conditions, the assumption of steady-state operation loses its relevance, and dynamic factors such as rotor-stator interaction (RSI), pulsation, inlet recirculation and cavitation have an increasing influence [18,29]. The complexity of the fluid flow structure in the flow path of centrifugal pumps, coupled with their importance for various industrial sectors, makes the simulation of the dynamic interaction between hydraulic forces and rotor design one of the central areas of the research in the field of pump reliability.

When using surrogate modelling methods for pump impellers, the resulting geometric models require experimental validation, especially when it comes to optimised shapes with complex geometry. It is extremely important to study the interaction between the fluid and the structure (FSI) during the operation of a centrifugal pump, especially for impellers without a shroud as well as prototypes of impellers created using additive technologies. An impeller optimised exclusively on the basis of hydrodynamic efficiency may have insufficient rigidity or natural frequencies that coincide with the blade pitch frequency, which will lead to resonance. Ignoring blade deformations under the action of hydrodynamic loads and centrifugal forces can distort the calculated geometry of the flow path, negating the results of optimisation. To verify the obtained geometry, an FSI analysis is performed, implemented directly into the optimisation cycle, considering vibrations [30] and stresses [16,31] as limiting factors or additional objective functions. This approach allows the creation of a pump design that not only has good energy characteristics but also structural reliability, enabling it to withstand intense dynamic loads.

Figure 1. Optimisation pipeline.

Mathematical modelling of FSI in turbomachinery is a complex multiphysics simulation task that requires simultaneous solution of equations describing fluid motion and structural deformation.

The flow is modelled using Navier-Stokes equations, specifically their Reynolds-averaged variant (Reynolds Navier-Stokes averaging, RANS), to account for the moving boundaries of the deforming impeller.

The RANS turbulence model is a statistical turbulence model due to the use of the corresponding averaging method used to formulate the equations. The application of averaging processes requires the introduction of additional unknown terms consisting of products of variable quantities that serve as additional stress factors in the fluid.

Given that the study was conducted under steady-state conditions, a turbulence model based on the Reynolds-Averaged Navier-Stokes (RANS) (Eq.1 and 2) equations was selected. This approach employs statistical averaging to derive the governing equations, which significantly reduces the computational resources needed [32–34].

$$\frac{\partial \overline{u_i}}{\partial x_j} = 0 \tag{1}$$

$$\overline{u_j}\frac{\partial \overline{u_i}}{\partial x_j} - \frac{\partial}{\partial x_j}\left[(\nu - \nu_T)\left(\frac{\partial \overline{u_i}}{\partial x_j} - \frac{\partial \overline{u_j}}{\partial x_i}\right)\right] + \frac{1}{\rho}\frac{\partial \overline{\tilde{p}}}{\partial x_j} = 0 \tag{2}$$

The monolithic approach solves the equations of fluid motion and structural deformation within a single mathematical model, ensuring strict conservation of energy at the interface and reliability for problems with a strong added mass effect, but due to its high computational cost, it is used less frequently. It should also be noted that the mechanical characteristics of materials used in additive manufacturing are characterised by small deformations, so in the case of this study, preference was given to a split approach, in which the fluid motion and structural deformation domains are solved separately and linked via boundary conditions at the interface.

Within the framework of the split approach, a one-way connection is used, which ignores the feedback of structural deformation with the flow field, which is sufficient for static stress analysis.

When using this method, the iterative feedback loop of the two-way connection is not taken into account, which significantly speeds up the process.

The choice of structural material for additive manufacturing of centrifugal pump impeller prototypes is dictated by the need to ensure sufficient specific strength and rigidity. As part of the digital research, a comparative analysis of the properties of three common thermoplastics was also carried out: polyamide-12 (PA-12 Industrial), acrylonitrile butadiene styrene (ABS) and polyethylene terephthalate glycol (PETG).

Most of the calculations presented were performed on PA-12 simulating the use of the selective laser sintering (SLS) method.

This material demonstrates a high degree of isotropy of mechanical properties and structural integrity. According to a study [35], sintered PA-12 samples are characterised by a tensile strength in the range of 45–50 MPa, which correlates with the manufacturer's declared value for the PA-12 Industrial material used (48.7 MPa) [36]. A key advantage of PA-12 is its ability to undergo plastic deformation before failure and its high impact strength, which is critical for preventing failure under pulsation loads resulting from rotor-stator interaction [37]. Unlike polyamides, materials used in extrusion technologies, such as ABS and PETG, exhibit pronounced anisotropy of properties depending on the orientation of the print layers [38].

2. Materials and Methods

A CH 100/32-11-1 centrifugal canned monoblock pump was selected as the base object for numerical modelling and verification. This unit belongs to the class of single-stage centrifugal pumps and is characterised by the following design parameters (Table 1).

Table 1

CH 100/32-11-1 (4) Pump parameters

Parameter	Designation	Value	Units
Nominal flow rate	Q_{nom}	100	m^3/h
Nominal head	H_{nom}	32	m
Working feed interval	Q_{op}	65...140	m^3/h
Permissible cavitation margin	$NPSH_r$	3.5	m
Nominal motor power	P_n	11.0	kW
Temperature of pumped liquid	T	-40...+40	°C
Cooling type	-	W/L (Air)	-

The CFD part of the study was performed in ANSYS CFX. A detailed full-scale hydraulic model was used for the CFD simulation, including the suction pipe, rotating impeller, and casing volute discharge. The stationary and rotating domains were connected via a common Frozen rotor interface to maintain mass and momentum conservation during the transition between frames. The exact implementation of the boundary conditions is schematically shown in Fig. 2.

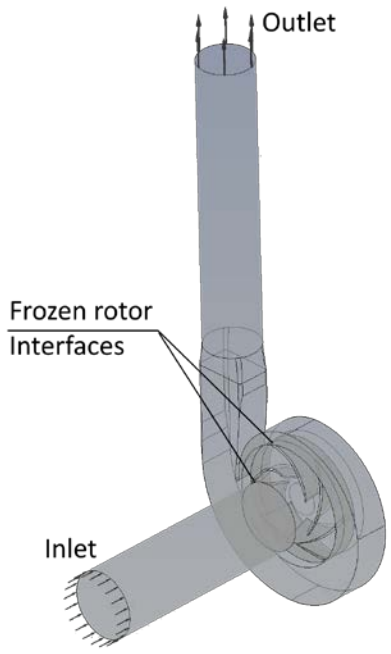

Figure 2. Geometric model with initial and boundary conditions specified.

The boundary condition at the Inlet was characterised by a total pressure condition P_{inlet} = 10 m. The inlet flow assumes a single-phase liquid water medium with a turbulence intensity of 1%, in accordance with recommendations for real pumping systems to obtain a stable upstream flow.

A mass flow boundary condition Q_{outlet} = 31 kg/s was set at the Outlet of the domain. For transport variables related to turbulence at the outlet, a zero gradient condition was implemented at the outlet of the calculation domain. The simulation was performed under isothermal conditions at a liquid temperature of 25 °C, with a reference pressure set at P_{ref}= 0 atm. A rotation speed of n = 2950 min^{-1} was specified for the impeller domain.

Due to significant computational costs and the formulation of the problem using the FSI one-way coupling model, the Reynolds-Navier-Stokes (RANS) equations were solved using a steady-state formulation. In this research, the SST (Menter's Shear Stress Transport) turbulence model, eq. (3) and (4), is used [39]:

$$\frac{\partial(\rho k)}{\partial t}+\frac{\partial\left(\rho u_j k\right)}{\partial x_j}=P-\beta^*\rho\omega k+\frac{\partial(\rho k)}{\partial x_j}\left[(\mu+\sigma_k\mu_t)\frac{\partial k}{\partial x_j}\right] \tag{3}$$

$$\frac{\partial(\rho\omega)}{\partial t}+\frac{\partial\left(\rho u_j\omega\right)}{\partial x_j}=\frac{\gamma}{v_t}P-\beta\rho\omega^2+\frac{\partial}{\partial x_j}\left[(\mu+\sigma_\omega\mu_t)\frac{\partial\omega}{\partial x_j}\right]+2(1-F_1)\frac{\rho\sigma_{\omega2}}{\omega}\frac{\partial k}{\partial x_j}\frac{\partial\omega}{\partial x_j} \tag{4}$$

where: xj represents the partial spatial coordinates, with the subscript j indicating the spatial directions (x, y, z), uj denotes the mean flow velocity components in the j- direction, k is the turbulent kinetic energy, ω represents the specific dissipation rate, μ is the dynamic viscosity, νt is the turbulent kinematic viscosity, μt is the turbulent (eddy) viscosity, ρ is the fluid density and P is the turbulence production term.

Convergence conditions were chosen to attain convergence while optimising computational resources. A finite total of 1000 iterations for calculations were designated, and the computations also conclude when a tolerance level for the root mean square residual error of 10^{-6} is attained. This method guarantees numerical convergence with reduced execution time. CFD calculation results are presented in Fig. 3.

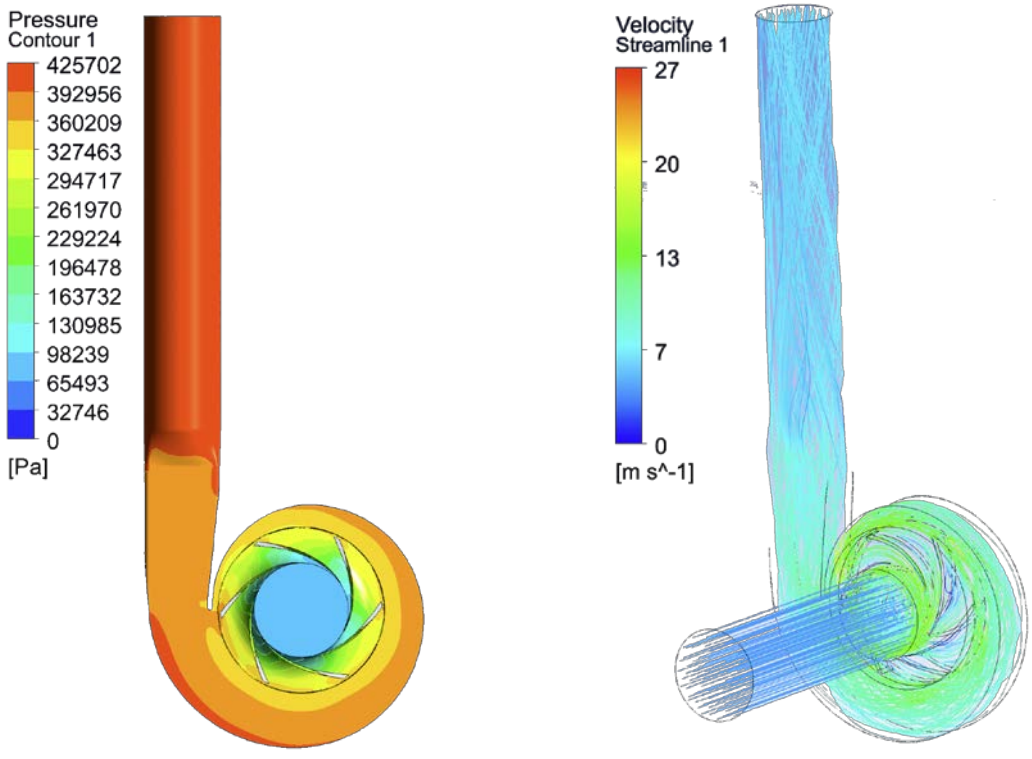

(a) (b)

Figure 3. Pressure field distribution and streamlines indicating flow velocity.

In the next stage of the study, the data obtained in the CFD simulation using the ANSYS Workbench platform was transferred to ANSYS Mechanical. The simulation area was limited to the impeller itself and its associated components, namely the shaft and bearings (Fig. 4). Simplifying the shaft and bearings is a common approach in such tasks, where the main focus is on the impeller design [30].

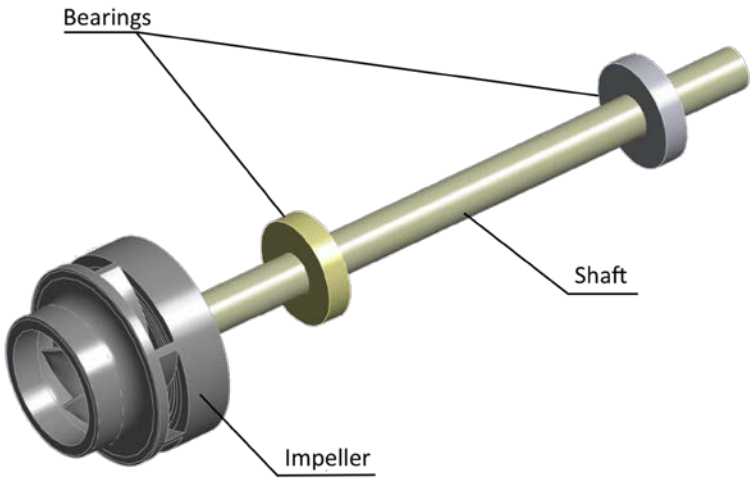

Figure 4. Geometric model used in FSI simulation.

A fragment of the discretised geometric model used in this calculation is shown in Fig. 5. To achieve an optimal compromise between computational efficiency and numerical accuracy, the shaft and bearing components were discretised using a maximum element size of ΔS = 2.5 mm. In contrast, the impeller, being a critical component with complex geometry, required a finer discretisation; a maximum element size of ΔS = 0.9 mm was applied to accurately solve the problem. In the final calculation, a grid with $9.037 \cdot 10^6$ elements was used.

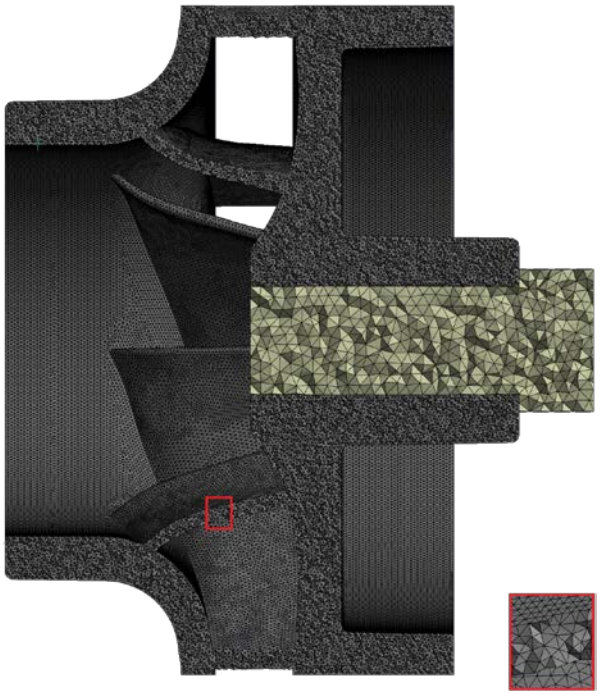

Figure 5. Discretisation model.

In order to verify the accuracy of the results obtained, a convergence analysis was performed. Its results are presented in Fig. 6. It can be noted that convergence was achieved for all parameters: deformation, displacement, and stress.

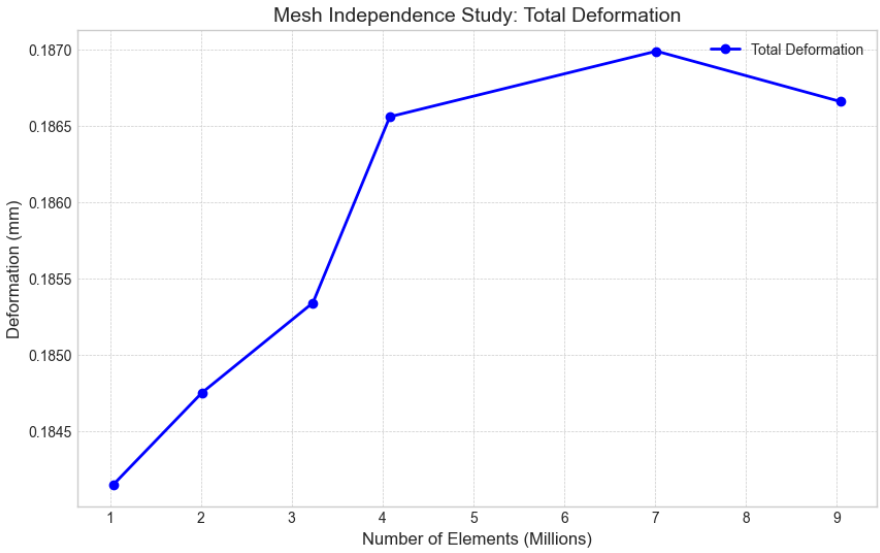

(a)

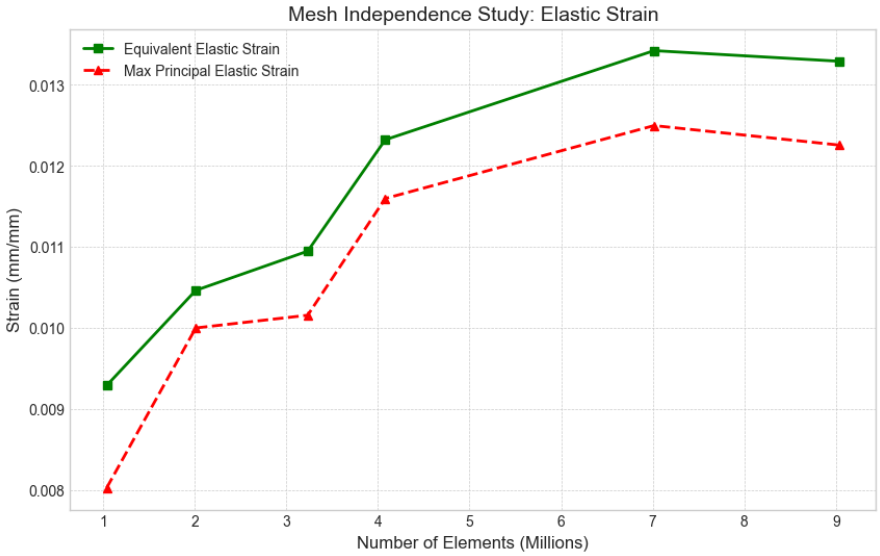

(b)

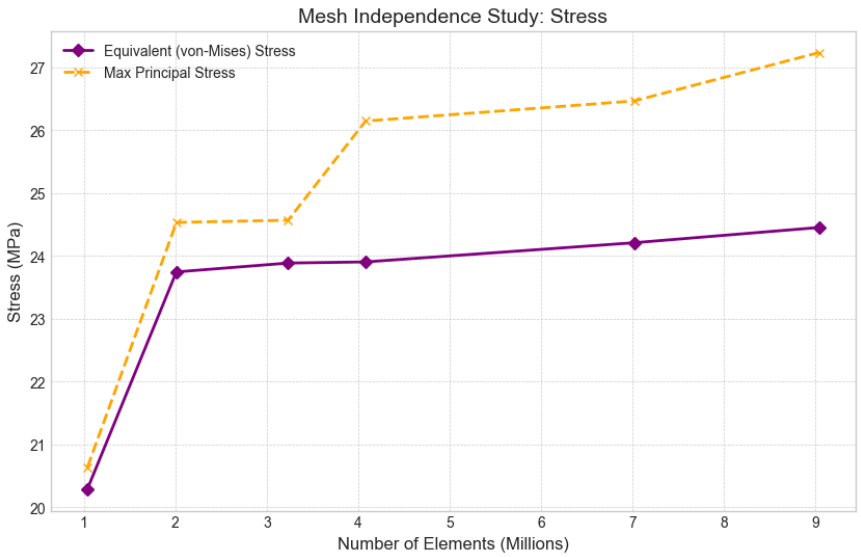

(c)

Figure 6. Convergence plots for: a) Deformation vs. Number of elements in mesh, b) Strain vs. Number of elements in mesh, c) Stress vs. Number of elements in mesh.

The study of stresses and deformations was carried out using the Transient-Structural module from ANSYS Mechanical. The calculation is based on the equation of motion of a linearly elastic body, which in matrix form (Eq. 5) is represented by the following mathematical model [40]:

$$M_s\ddot{u} + C_s\dot{u} + K_s u = F_s\,, \tag{5}$$

where: u denotes the displacement vector, $\dot{u}$ - velocity vector, $\ddot{u}$ - acceleration vector, M_s - the mass matrix, C_s - damping matrix, K_s - stiffness matrix and F_s represents the applied vector.

Considering the equivalent stiffness of the link, we derived the Eq.6 [31]:

$$M_s\ddot{u} + C_s\dot{u} + K_s u + K_{fs}p = F_s\,, \tag{6}$$

where:$K_{fs} = -R$ represents the equivalent stiffness and p denotes the fluid pressure.

3. Results

The calculation results show that the equivalent stress reaches 24.45 MPa, which is still less than the tensile strength of the PA-12 Industrial material (48.7 MPa). It should also be noted that the deformations are within the normal range. This means that this impeller prototype can be produced using the SLS method and tested for hydraulic characteristics (Fig. 7).

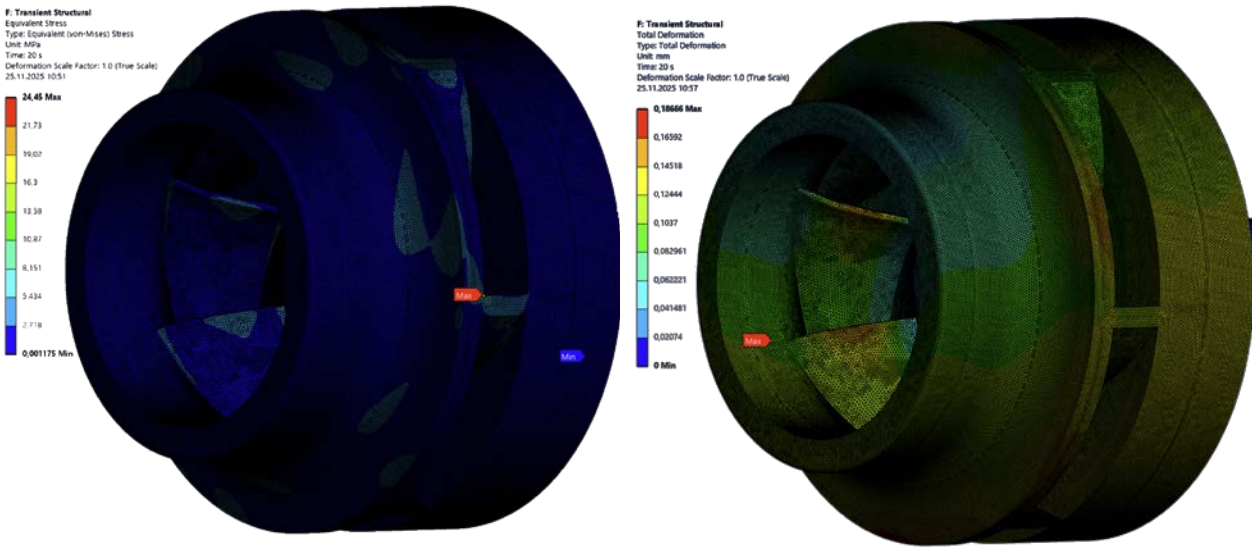

Figure 7. Simulation results for pump CH 100/32-11-1.

Using a similar pipeline, the results for two more pumps, CH 6.3/20-1.1-2 and CH 100/125-75-5, were analysed. The parameters of these two pumps are presented in Table 2.

Table 1

Pump characteristics

Model	CH 6.3/20-1.1-2	CH 100/32-11-1	CH 100/125-75-5
Nominal flow rate Q_{nom} , m^3/h	6.3	100	100
Nominal head H_{nom}, m	20	32	125
Motor power N, kW	1.1	11	75
Specific speed, n_q	13	36.5	13.2

In the case of the CH 6.3/20-1.1-2 pump, the equivalent stress was 11.809 MPa, which allows the prototype of this impeller made of PA-12 to be used in bench tests, but for the CH 100/125-75-5 pump, the equivalent stress was already 51.7 MPa, a value that exceeds the strength limit of this material (Fig. 8).

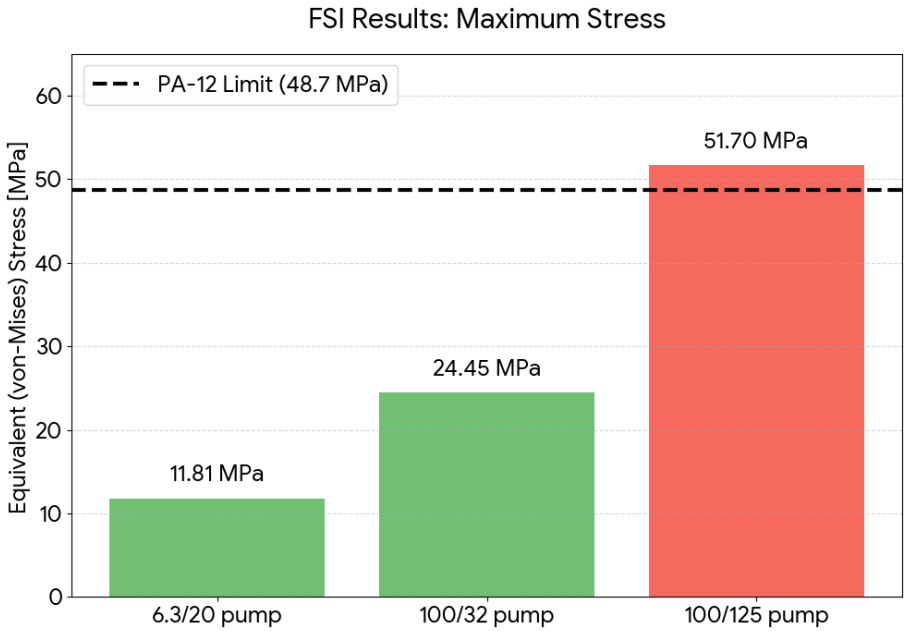

Figure 8. Equivalent stress values obtained during FSI simulation.

If we analyse and compare the stress distribution in the CH 100/32-11-1 pump impeller with the distribution obtained for the CH 100/125-75-5 pump (Fig. 9), we can see that the stress pattern is similar. The area with the highest stress is the outer part of the impeller. It should also be noted that the main stress concentrator is located at the blade outlet in the area of the junction with the hub and shroud surfaces.

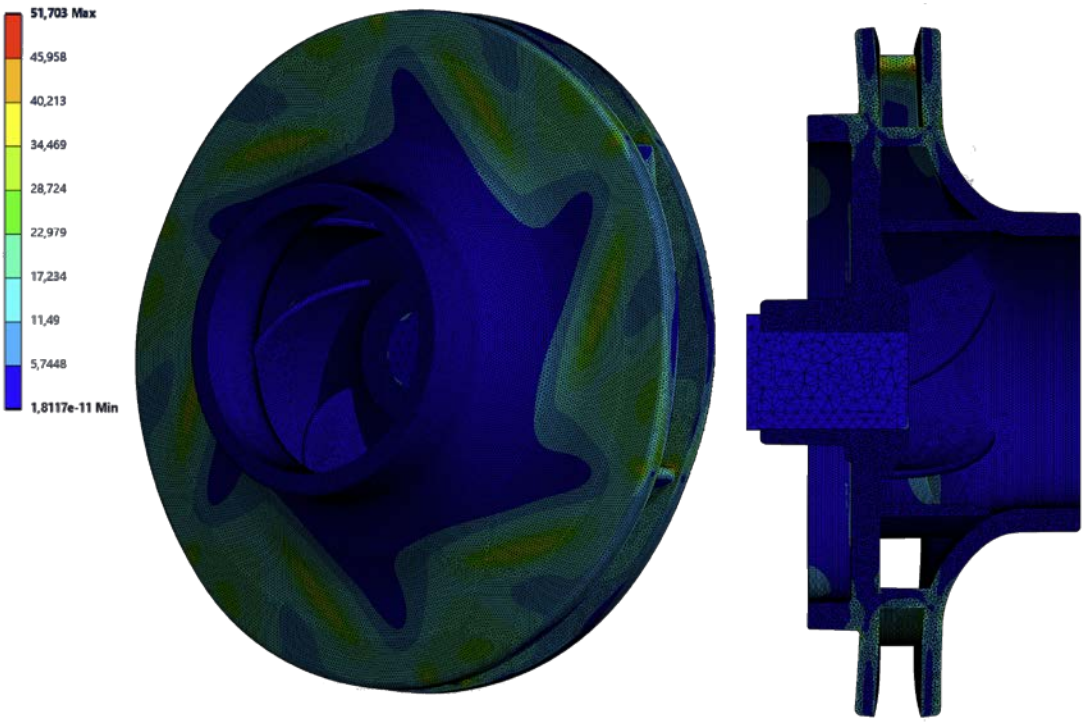

Figure 9. Stress distributions obtained in simulations for pump CH 100/125-75-5.

4. Discussion

The data obtained in the study are important for developers of this type of pump in the Republic of Moldova and can be used in optimisation cycles to obtain new pump components, with the aim of expanding the range of centrifugal pumps and thus increasing the competitiveness of enterprises producing centrifugal pumps in Moldova. As a direction for further research, the authors plan to continue developing a line of centrifugal pumps with different parameters, incorporating FSI simulation into the optimisation cycle.

5. Conclusions

This study successfully demonstrates the application of a joint CFD/FEA workflow to verify the structural integrity of impeller prototypes intended for additive manufacturing using PA12 Industrial.

The results obtained for the CH 100/32-11-1 pump confirm the suitability of PA12 material for this specific hydraulic specification. Numerical results indicate a maximum equivalent stress of 24.45 MPa under nominal operating conditions. When compared to the material's tensile strength limit of 48.7 MPa, this gives a safety factor of approximately 2.0. The CH 100/32-11-1 prototype has been tested for structural reliability for production using SLS technologies and subsequent experimental verification of its hydraulic characteristics.

A comparative analysis was performed for pumps of different sizes, which highlights the limitations of the application of this material. While the CH 6.3/20-1.1-2 model demonstrated a maximum equivalent stress value of 11.8 MPa, which is significantly below the critical threshold, the larger CH 100/125-75-5 model demonstrated the limits of the polymer's application. In the latter case, the equivalent stress reached 51.7 MPa, exceeding the structural capacity of the industrial material PA12. This fact represents a non-linear relationship between pump size, hydraulic power and structural load and serves as evidence of the need to use FSI simulation in the optimisation cycle.

The resulting stress distribution is uneven, but similar in shape for all three pumps. Critical stress concentration zones are invariably located at the rear edge of the blade, in particular at the joints with the surfaces of the impeller's hub and shroud. This localization is explained by the superposition of the centrifugal forces of the body and the maximum pressure difference occurring at the outlet of the impeller. Thus, the presented numerical model confirms the possibility of using PA12 Industrial for prototyping impellers using CFD/FSI simulation to evaluate mechanical properties.

Acknowledgments: This research is financially supported by the National Agency for Research and Development, research programme: "Young researchers", Financing agreement no. 159TC. "Optimising the energy efficiency of centrifugal pumps using CFD methods and algorithms based on Artificial Intelligence." Period: 2025-2026

Conflicts of Interest: The authors declare no conflict of interest.

References

1. Yuan, J., Shi, J., Fu, Y., Chen, H., Lu, R. & Hou, X. (2022) Analysis of fluid-structure coupling dynamic characteristics of centrifugal pump rotor system. *Energies,* 15, 2133.
2. Bogdanovic-Jovanovic, J., Stamenkovic, Z., Kocić, M. & Petrović, J. (2024) Performance prediction of centrifugal norm pumps operating as turbines. *Fluids,* 9, 190.
3. Renzi, M. & Rossi, M. (2019) A generalized theoretical methodology to forecast flow coefficient, head coefficient and efficiency of pumps-as-turbines (PaTs). Vol. 158, p. 134.

4. Bostan, V. & Petco, A. (2023) Study of the empirical models' applicability for calculating the centrifugal pump's impellers geometric parameters. *Journal of Engineering* Science, pp. 8–22.
5. Bostan, V. & Petco, A. (2024) Design and optimization of the centrifugal pump impeller for wastewater. Vol. 46, pp. 362–369.
6. Liu, H., Jiang, L., Wang, Y., Hočevar, M., Yan, J. & Chen, J. (2022) Optimization and CFD performance analysis of an automotive coolant pump. *Advances in Mechanical Engineering*, 14, 168781322210816.
7. Malael, I. & Gherman, G.B. (2018) Numerical investigation of a new LH2 centrifugal pump concept used in space propulsion. *INCAS Bulletin*, 10, 65–74.
8. Ciucci, M. (2023) Politica energetică: principii generale. Available online: https://eur-lex.europa.eu/legal-content/RO/TXT/PDF/?uri=CELEX:32023L1791 (Accessed: 15.11.2025).
9. Document de reflecție (2019) Către o Europă durabilă până în 2030. Available online: https://eur-lex.europa.eu/legal-content/RO/TXT/PDF/?uri=CELEX:32023L1791 (Accessed: 15.11.2025).
10. Stroncea, A., Toca, A. & Nițulenco, T. (2023) Considerations regarding the optimal dimensional design of machining technologies. *ACTA TECHNICA NAPOCENSIS - Series: Applied Mathematics, Mechanics, and Engineering*, 66.
11. Mazuru, S. & Scaticailov, S. (2023) New technological solution for manufacturing precessional gears with non-standard profile. *ACTA TECHNICA NAPOCENSIS - Series: Applied Mathematics, Mechanics, and Engineering*, 66.
12. Kim, B., Siddique, M.H., Samad, A. & Lee, D.-E. (2022) Optimization of centrifugal pump impeller for pumping viscous fluids using direct design optimization technique. *Machines,* 10, 774.
13. Górecki, J., Klimentov, K., Popov, G., Kostov, B. & Ibrahim, S. (2024) Studying the impact of diffuser return guide vanes on the energy performance of a multistage centrifugal pump. *Applied Sciences,* 14, 10991.
14. Kaya, D., Yagmur, E.A., Yigit, K.S., Kilic, F.C., Eren, A.S. & Celik, C. (2008) Energy efficiency in pumps. *Energy Conversion and Management*, 49, 1662–1673.
15. National Renewable Energy Laboratory (NREL) (n.d.) Pump life cycle costs: A guide to LCC analysis for pumping systems: Executive summary. Available online: https://docs.nrel.gov/docs/fy01osti/29084.pdf (Accessed: 15.11.2025).
16. Arocena, V.M. & Danao, L.A.M. (2023) Improving the modeling of pressure pulsation and cavitation prediction in a double-volute double-suction pump using mosaic meshing technology. *Processes,* 11, 660.
17. Li, Y., Feng, G., Li, X., Si, Q. & Zhu, Z. (2018) An experimental study on the cavitation vibration characteristics of a centrifugal pump at normal flow rate. *Journal of Mechanical Science and Technology*, 32, 4711–4720.
18. Bostan, V. & Petco, A. (2025) Analysis of cavitation phenomenon as a criterion for optimization of centrifugal pump design. *ACTA TECHNICA NAPOCENSIS - Series: Applied Mathematics, Mechanics, and Engineering*, 68.
19. Gülich, J.F. (2020) Centrifugal Pumps. Cham: *Springer International Publishing*.
20. Lobanoff, V.S. & Ross, R.R. Centrifugal Pumps: Design and Application. Available online: https://www.abebooks.com/9780872012004/Centrifugal-Pumps-Design-Application-Lobanoff-087201200X/plp (Accessed: 15.11.2025).
21. Xu, K., Wang, G., Wang, L., Yun, F., Sun, W., Wang, X. & Chen, X. (2020) Parameter analysis and optimization of annular jet pump based on Kriging model. *Applied Sciences*, 10, 7860.
22. Drăgan, V., Dumitrescu, O., Dobromirescu, C. & Popa, I.F. (2024) Satellite thermal management pump impeller design and optimization. *Inventions,* 9, 54.
23. Bostan, V. & Petco, A. (2024) Minimizing blade-fluid energy losses in centrifugal hydraulic pump impellers. *ACTA TECHNICA NAPOCENSIS - Series: Applied Mathematics, Mechanics, and Engineering*, 67.
24. Cao, W., Wang, H., Yang, X. & Leng, X. (2023) Optimization of guide vane centrifugal pumps based on response surface methodology and study of internal flow characteristics. *Journal of Marine Science and Engineering*, 11, 1917.
25. Pagayona, E. & Honra, J. (2024) Multi-criteria response surface optimization of centrifugal pump performance using CFD for wastewater application. *Modelling,* 5, 673–693.
26. Shojaeefard, M.H., Hosseini, S.E. & Zare, J. (2019) CFD simulation and Pareto-based multi-objective shape optimization of the centrifugal pump inducer applying GMDH neural network, modified NSGA-II, and TOPSIS. *Structural and Multidisciplinary Optimization*, 60, 1509–1525.
27. Zhang, J., Zhu, H., Yang, C., Li, Y. & Wei, H. (2011) Multi-objective shape optimization of helico-axial multiphase pump impeller based on NSGA-II and ANN. *Energy Conversion and Management*, 52, 538–546.
28. Bostan, V., Petco, A. & Șaragov, I. (2023) Empirical models' applicability for calculating the centrifugal pump's impellers geometric parameters. *Journal of Engineering Science*, 30, 8–19.

29. Shen, Z., Wang, C., Zhang, J., Qiu, S. & Lin, R. (2024) Study on part-load cavitation in high-specific-speed centrifugal pump. *Water,* 16, 2180. doi:10.3390/w16152180.
30. Yuan, J., Shi, J., Fu, Y., Chen, H., Lu, R. & Hou, X. (2022) Analysis of fluid-structure coupling dynamic characteristics of centrifugal pump rotor system. *Energies,* 15, 2133.
31. Yin, T., Pei, J., Yuan, S., Osman, M., Wang, J. & Wang, W. (2017) Fluid-structure interaction analysis of an impeller for a high-pressure booster pump for seawater desalination. *Journal of Mechanical Science and Technology*, 31, 5319–5328.
32. Nonino, M., Ballarin, F. & Rozza, G. (2021) A monolithic and a partitioned, reduced basis method for fluid–structure interaction problems. *Fluids,* 6, 229.
33. Benra, F.-K., Dohmen, H., Pei, J. & Schuster, S. (2011) A comparison of one-way and two-way coupling methods for numerical analysis of fluid-structure interactions. *Journal of Applied Mathematics*.
34. Li, W., Ji, L., Shi, W., Zhou, L., Jiang, X. & Zhang, Y. (2016) Vibration characteristics of the impeller at multi-conditions in mixed-flow pump under the action of fluid-structure interaction. *Journal of Vibroengineering*, 18, 3213–3224.
35. Goodridge, R.D., Tuck, C.J. & Hague, R.J.M. (2012) Laser sintering of polyamides and other polymers. *Progress in Materials Science,* 57, 229–267.
36. Sinterit (n.d.) PA12 Industrial Powder | Polyamide 12 for 3D Printing | Sinterit. Available online: https://sinterit.com (Accessed: 15.11.2025).
37. Greiner, S., Wudy, K., Lanzl, L. & Drummer, D. (2017) Selective laser sintering of polymer blends: Bulk properties and process behavior. *Polymer Testing*, 64, 136–144.
38. Tymrak, B.M., Kreiger, M. & Pearce, J. (2014) Mechanical properties of components fabricated with open-source 3-D printers under realistic environmental conditions. *Materials & Design,* 58, 242–246.
39. Menter, F.R. (1994) Two-equation eddy-viscosity turbulence models for engineering applications. *AIAA Journal*, 32, 1598–1605.
40. Fu, Y., Yuan, J., Yuan, S., Pace, G., d'Agostino, L., Huang, P. & Li, X. (2015) Numerical and experimental analysis of flow phenomena in a centrifugal pump operating under low flow rates. *Journal of Fluids Engineering*, 137, 011102.

Citation: Bostan, V., Petco, A., Odainii, D., Croitor, D., Zubac, V., Proca, N. (2026). Application of fluid-structure interaction simulations in the optimisation cycle of centrifugal pump impellers. *Journal of Engineering Science*. 2026, 33 (1), pp. 8-20. https://doi.org/10.52326/jes.utm.2026.33(1).01.

Submission of manuscripts: jes@meridian.utm.md